Time variant de-ghosting and its applications in WAZ data

Zhigang Zhang, Zhaohong Wu, Bin Wang, and Jean Ji, TGS, Houston, TX, USA*

Summary

The importance of de-ghosting cannot be overstated in the pursuit of a broad-band image, and an accurate estimation of the ghost delay time, explicitly, or implicitly, is critical for the de-ghosting process. We propose the uses of L2 or L1 norm of the de-ghosted data in search of the ghost delay time. This method has proven robust and stable using both synthetic data and real data. We have built a time-variant adaptive de-ghosting method with this method, applied it for wide azimuth (WAZ) and full azimuth (FAZ) data, and provide results in this abstract. The proposed method has the capability to handle uncertainties in receiver depth and water velocity, and 3D effects, which makes it practical to apply.

Introduction

A high resolution image requires a narrow wavelet, which can be translated into a broad spectrum in the frequency domain. This endeavor is constrained by the existence of both source and receiver ghosts, the reflection of up-going wave from the water surface in marine acquisitions. Ghosts closely follow the primaries in seismic data with opposite polarity. Interference between the ghosts and primaries enhances energy in some frequencies while attenuates energy in others, including the much desired low frequencies.

Research to separate the ghost and primary can be tracked back decades ago (*Jovanovich et al., 1983*), but practical applications were much limited until recently substantial progress was made in both acquisition methods and processing algorithms. Implementations of slant cable (*Soubaras, 2010, 2012*) and dual depth streamer (*Posthumus, 1993*) take advantage of receiver notch diversity brought by the variable receiver depth. Multi-sensor design, on the other hand, recovers lost information in the hydrophone with signals from other sensors, such as the geo-phones (*Carlson et al., 2007*). Though these acquisition-based methods are very successful, research of processing-based de-ghosting algorithms for conventional data acquisition receives great interest because of the obvious benefit from de-ghosting and wide availability of legacy data (*Baldock et al., 2012; Robertsson et al., 2014; Telling et al., 2014; Wang et al., 2013; Zhou et al., 2012*).

Successful processing-based de-ghosting requires accurate knowledge of the ghost delay time, which is the time gap between the primary and ghost. The ghost delay time is a function of the emerging angle of the up-going wave, receiver or source depth, and water velocity. The tau-*p* transform plays an important role in most de-ghosting algorithms (*Masoomazadeh et al., 2013; Robertsson et al., 2014; Telling et al., 2014; Wang et al., 2013*). It decomposes wave field into local plane wave which has a uniform emerging angle everywhere along the streamer. But because of the sparse sampling in the cross-line direction and high cost of an inversion based 3D tau-*p* transform, most current algorithms utilize 2D tau-*p* transform.

There are many reasons that can cause a 2D de-ghosting algorithm go wrong. The 3D effect, such as reflections from off-plane events, results in time variant ghost delay time even for the same p_x. The uncertainties in receiver depth due to bad weather and inaccuracy of water velocity are all very common in practice and may also leave ringing in the de-ghosted data. To be successful, a de-ghosting algorithm must adapt itself to these scenarios. Sometimes different algorithms are required for different data sets.

WAZ and FAZ acquisitions pose additional challenges. Firstly, the slowness in the cross-line direction (p_y) is mostly not zero, which invalidates the 2D assumption. Though this difficulty could be alleviated by using the real offset between the source and receivers in the tau-*p* transform and calculating the slowness in the radial direction (p_r), the challenge is not solved. Secondly, the irregular offset distribution increases the cost of tau-*p* transform. Compounding the issue, guns are positioned to the side of some cables with substantial distance resulting in small offset changes as the azimuth approaches 90 degree. Even a very small event dip can result in a very large slowness value because of the fine offset distribution. Last but not least, the source signature is directional. Sometimes, source brings in an inherent notch in the frequency spectrum close to the ghost notch and makes QC and de-ghosting more difficult.

A natural choice to handle the 3D effect and irregular offset distribution is to design a time-variant de-ghosting algorithm, which can adaptively accomplish search and de-ghost in small windows. Such a strategy requires a stable and robust search algorithm for the ghost delay time, since geology effect becomes prominent in small windows and many statistical methods lose their stability. A reliable tau-*p* transform is also critical for the de-ghosting purpose to more accurately group energy with the same ghost delay time.

Recently, an inversion based 3D tau-*p* transform method has been proposed and shown great results (*Wang et al., 2014; Wu et al., 2014*). This method applies a sparse

DOI http://dx.doi.org/10.1190/segam2015-5926545.1

constraint to reduce the computation cost and surpasses the limit set by sparse sampling in the cross-line direction. In this abstract, we propose an alternative algorithm to de-ghost WAZ and FAZ data. We firstly design an adaptive ghost delay time searching algorithm and then use it to build a time-variant de-ghosting procedure. We also use a high resolution tau-*p* transform and accomplish de-ghosting in the tau-*p* domain. Our tests using synthetic and real data have shown the algorithm is very robust.

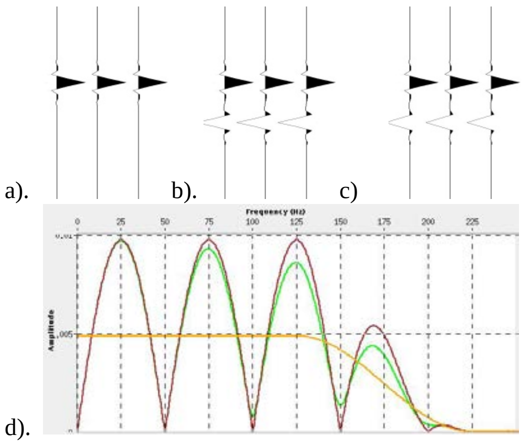

Figure 1. Wavelet and spectrum with and without ghost. a) Input wavelet without a ghost; b) Ghosted wavelet using ghost operator in equation (4); c) Ghosted wavelet using ghost operator in equation (3); d) Amplitude spectrum of input wavelet (yellow), wavelet in b) (red), and wavelet in c) (green). The ghost delay time equals 20ms. In equation 3), the parameter σ=240Hz, which is equivalent to about 1m of rms wave height.

A time variant de-ghosting algorithm

Though mostly treated as negative one, the reflection coefficient at the water-air interface is actually a function of frequency, emerging angles, and wave conditions (*Jovanovich et al., 1983*). It decreases from low to high frequency, and as a result the ghost notch always becomes shallower in high frequency in real data. In this abstract, we use a Gaussian type function for the reflection coefficient, as

$$r(f) = e^{-\frac{1}{\sigma^2}f^2}, \quad (1)$$

where σ is a positive number. This is a simplification of the formula used by Jovanovich that ignores the wave directions. In the frequency domain, the ghost operator then could be written as

$$G(f) = 1 - r(f)e^{-i2\pi f\Delta}, \quad (2)$$

where Δ is the true ghost delay time. We can easily find its impulse response in continuous time domain as

$$g(t) = \delta(t) - \sigma\sqrt{\pi}e^{-\sigma\pi^2(t-\Delta)^2}. \quad (3)$$

When σ is very large, $r(f)$ is close to 1 and both the frequency domain operator and time domain pulse response converge to their calm water surface cases, respectively. Specifically, the ghost operator changes to

$$G(f) = 1 - e^{-i2\pi f\Delta}. \quad (4)$$

Figure 1 shows the wavelet and amplitude spectrum of a broad band wavelet without ghost and after applying a ghost operator. The sample time is 2ms and there is only very subtle difference between the two operators given by (3) and (4).

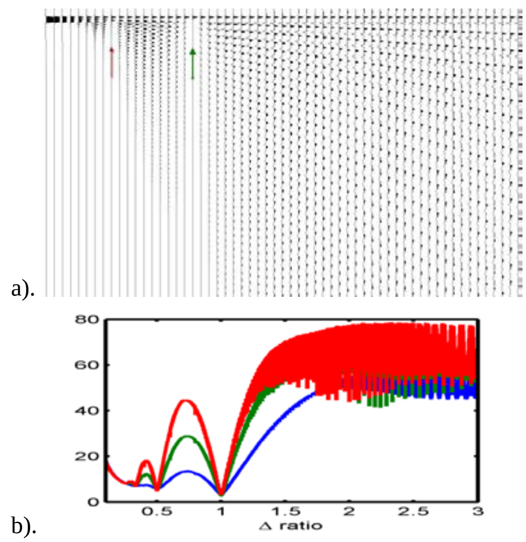

Figure 2. Effect of Δ_a on de-ghosting. a) De-ghosted data with different Δ_a, from left to right, Δ_a changes from 2ms to 60ms. Perfect de-ghosting is achieved when $\Delta_a = \Delta$ (green arrow). When $\Delta_a = 0.5\Delta$ (red arrow), the primary is followed by another peak with the same polarity and amplitude at 10ms in the de-ghosted data; b) The L1 norm of the de-ghosted data. The x axis is the ratio Δ_a/Δ. Curves of different σ are displayed in different color, with green for σ=240Hz, which is the true value, red for σ=480Hz, and blue for σ=120Hz.

Ghost can be eliminated in either frequency domain or time domain (*Robertsson et al., 2014*). In our tests, we apply the following de-ghosting operator in frequency domain,

$$F(f) = \frac{1}{1-r(f)e^{-i2\pi f\Delta_a}}. \quad (5)$$

We use Δ_a to denote the actual delay time we use. In frequency domain, the de-ghosted data, denoted as $P_{dg}(f)$, can then be written as

DOI http://dx.doi.org/10.1190/segam2015-5926545.1

$$P_{dg}(f) = \frac{1-r(f)e^{-i2\pi f\Delta}}{1-r(f)e^{-i2\pi f\Delta_a}}P(f), \quad (6)$$

where $P(f)$ is the true primary without ghost. The de-ghosting operator compensates the ghost operator and recovers the primary accurately when both the delay time Δ and $r(f)$ are known. Incorrect time delay Δ_a causes ringing in the data. In frequency domain, it boosts energy in the wrong frequency and the total energy increases. This fact inspires us to use the total energy of de-ghosted data to search the true delay time Δ.

Figure 2 demonstrates how the L1 norm of the de-ghosted data changes with Δ_a. The input signal is shown in Figure 1c with σ=240Hz, with ghost delay time equal to 20ms, and centered in a 2s time window. We scan Δ_a from 2ms to 60ms, equivalent from 0.1Δ to 3Δ, a very large range. When $\Delta_a = \Delta$, the primary is correctly recovered. Larger Δ_a causes ringing and the L1 norm of $P_{dg}(t)$ increases rapidly. Round-up appears after about 1.5Δ because of the limited window size, and causes "lion tail" in the L1 curve, but it does not affect the optimization. A local minimum occurs at 10ms, half of the real delay time, with the objective function about twice as much as the global minimum.

In practice, we mostly have a rough estimation of Δ, especially in the tau-*p* domain, and the search range can be much smaller than what is shown in Figure 2, mostly between 0.5Δ to 1.2Δ. This makes the searching even more robust. We do not need an accurate estimation of σ. It affects the shape of the objective function, but does not change the location of minimum. Figure 2b shows how the objective function changes with σ. An additional search of σ may be applied later to further improve the result.

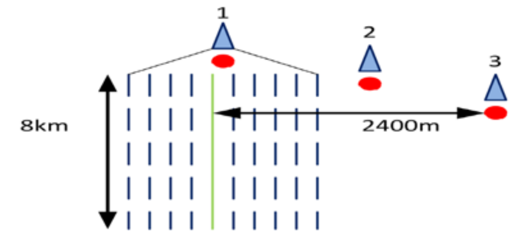

Figure 3. Gun-cable configuration. The acquisition utilizes 5 vessels. Only three are shown here because of limited space. The data used in this abstract is acquired using gun 3 and the cable in solid line. Cable length is about 8km, and the distance between the gun and cable is about 2400m.

We have tested different criteria in the search of delay time, including auto-correlation, amplitude spectrum, and phase spectrum. These methods need enough data to reduce the influence from noise and geology, and become unstable for small windows. Wang et al. (*2013*) propose to search Δ in the tau-*p* domain by minimizing an objective function which matches the primary and ghost. But it needs a set of mirror data, which is sometime not available or hard to obtain. Based on our observation, we suggest using the L1 norm of $P_{dg}(t)$ and solving the following optimization problem

$$\min_{\Delta_a^{min}<\Delta_a<\Delta_a^{max}} \left|P_{dg}(t)\right|_{L1} \quad (7)$$

where $P_{dg}(t)$ is the de-ghosted data in time domain, and $[\Delta_a^{min}, \Delta_a^{max}]$ is a range specified by the user. We use global search to avoid running into local minimums. Tests show L1 norm is more stable than L2 norm in real data.

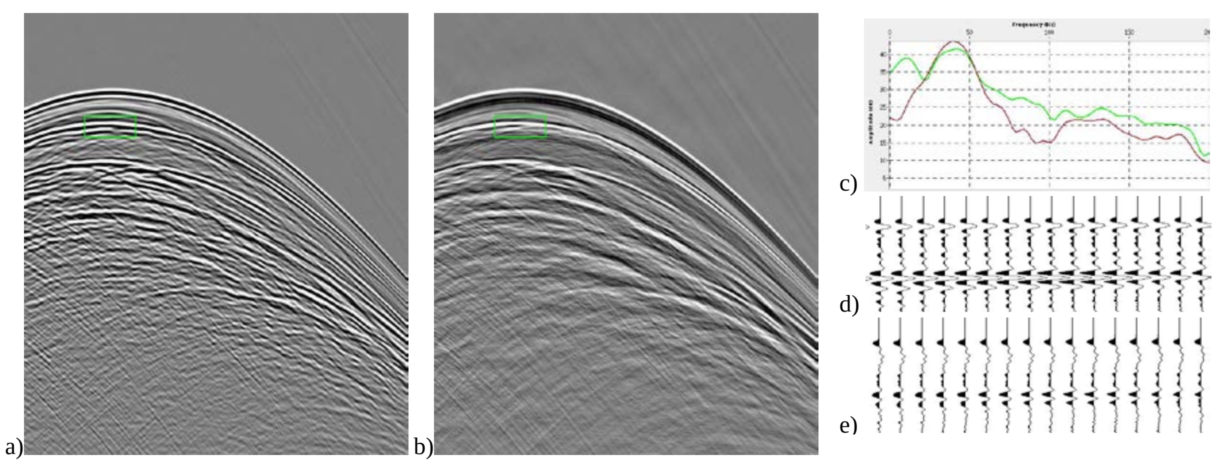

Figure 4. A shot gather before and after de-ghosting from a FAZ acquisition. a) Input data before de-ghosting; b) After both source and receiver de-ghosting; c) Amplitude spectrum of the region in the green box of input (red) and de-ghosted data (green); d) Wavelet of water bottom before de-ghosting; e) Wavelet of water bottom after de-ghosting

DOI http://dx.doi.org/10.1190/segam2015-5926545.1

Since the method is an adaptive method, the same strategy could be used for either source ghost, receiver ghost, or a combination.

We take advantage of a high resolution tau-*p* transform and apply de-ghosting in the tau-*p* domain. Our high resolution tau-*p* transform separates energy with different emerging angles well and makes it feasible to search in small windows. It also provides estimation for a good initial value and range for search.

Application in a FAZ acquisition

We have applied our time variant de-ghosting method to a FAZ data set in the Gulf of Mexico. The acquisition has a staggered configuration as partially shown in Figure 3. Positions of the gun and the cable used in this example are also shown. The source depth is fixed at 10m and the cable is towed flat at 12m. The cross-line distance between the gun and cable is about 2.4km. Near the point where the azimuth is close to 90 degree, the smallest offset change from one receiver to a neighbor receiver is about 0.03m. The offset is regularized before tau-*p* transform. We also make sure the input could be honestly recovered by an inverse transform without losing weak events or steep events.

Figure 4 shows a shot gather before and after de-ghosting on both source and receiver sides. Ghost energy is strongly attenuated. The high resolution tau-*p* transform separates the crossing events nicely and makes the adaptive de-ghosting successful, including diffractions and crossing events. Amplitude spectrum further confirms the de-ghosting results.

An NMO is then applied and the stacked images are shown in Figure 5a and 5b for comparison. The amplitude spectra are also shown in Figure 5c. The de-ghosting results are obvious in both stacked images and the flattened spectrum. Much clearer details can be seen in the de-ghosted image. Though there is still some notch residual, it could be removed by using other statistical methods (*Masoomazadeh et al., 2013*).

Conclusions and discussions

Rather than a 3D tau-*p* transform, we use a high resolution 2D tau-*p* transform. To compensate the 3D effect in WAZ and FAZ data, we propose the use of the L1 norm of the de-ghosted data as a search criterion for the ghost delay time in small windows. On this basis, we build a time variant de-ghosting procedure. This strategy turns out to be very successful. Our method can also be used in NAZ data with uncertainties in receiver depth or with mild 3D effect.

The search for ghost delay time is accomplished in small windows. In each window, the variance of delay time must be limited. Otherwise, ringing or some other artifacts will appear and force the de-ghosting to be less aggressive. Thus, a good method to group events according to their emerging angles is critical. In extreme cases, more sophisticated algorithms are still needed to achieve satisfactory results.

Acknowledgements

The authors wish to thank TGS for permission to include the Declaration data in this abstract. We are also grateful to Sampad Laha and Hasson Masoomzadeh for inspiring discussions, Connie VanSchuyver and Christopher Egger for proofreading the paper, and Roy Camp and James Espinosa for preprocessing the data.

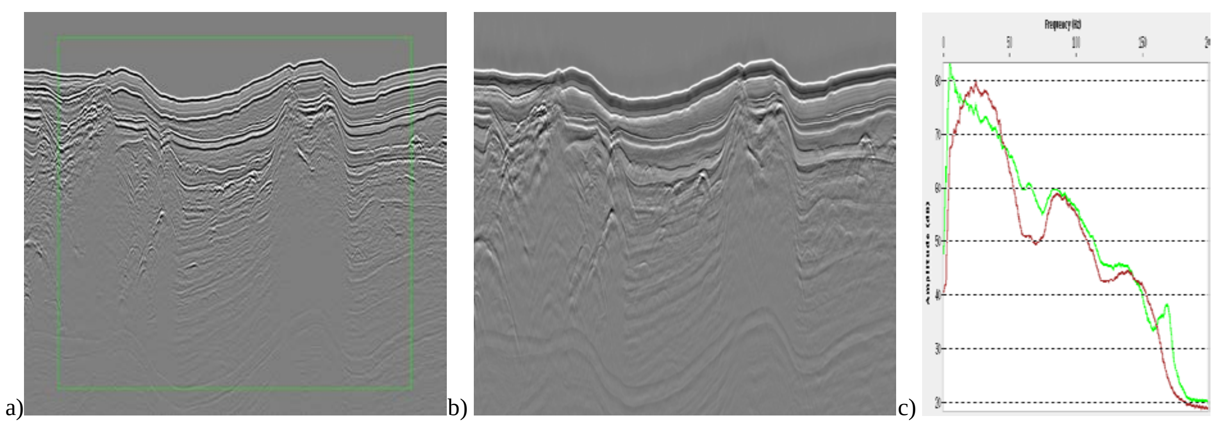

Figure 5. Comparison of stacked image before and after de-ghosting. a) Input data; b) After de-ghosting on both source and receiver sides; c) Amplitude spectrum from the region in the green box. Spectrum for the input data is show in red, while spectrum for the de-ghosted data is shown in green.

EDITED REFERENCES

Note: This reference list is a copyedited version of the reference list submitted by the author. Reference lists for the 2015 SEG Technical Program Expanded Abstracts have been copyedited so that references provided with the online metadata for each paper will achieve a high degree of linking to cited sources that appear on the Web.

REFERENCES

Baldock, S., N. Myziuk, H. Masoomzadeh, A. Hardwick, T. Travis, and N. Woodburn, 2012, Bringing broadband to the subsea: Oilfield Technology, **9**, 43–45.

Carlson, D. A., W. Long, H. Tobti, R. Tenghamn, and N. Lunde, 2007, Increased resolution and penetration from a towed dual-sensor streamer: First Break, **25**, 71–77.

Jovanovich, D. B., R. D. Sumner, and S. L. Akins-Easterlin, 1983, S.L., Ghosting and marine signature deconvolution, a prerequisite for detailed seismic interpretation: Geophysics, **48**, 1468–1485. http://dx.doi.org/10.1190/1.1441431.

Masoomzadeh, H., and N. Woodburn, Broadband processing of conventional streamer data-optimized deghosting in the Tau-P domain: 75th Annual International Conference and Exhibition, EAGE, Extended Abstracts, http://dx.doi.org/10.3997/2214-4609.20130093.

Posthumus, B. J., 1993, Deghosting using a twin streamer configuration: Geophysical Prospecting, **41**, no. 3, 267–286. http://dx.doi.org/10.1111/j.1365-2478.1993.tb00570.x.

Robertsson, J., L. Amundsen, and Ø. Pedersen, 2014, Deghosting of arbitrarily depth-varying marine hydrophone streamer data by time-space domain modeling: 84th Annual International Meeting, SEG, Expanded Abstracts, 4248–4252.

Soubaras, R., 2010, Deghosting by joint deconvolution of a migration and a mirror migration: 80th Annual International Meeting, SEG, Expanded Abstracts, 3406–3410.

Soubaras, R., 2012, Prestack deghosting for variable-depth streamer data: 74th Annual International Conference and Exhibition, EAGE, Extended Abstracts, I019.

Telling, R., N. Riddalls, A. Azmi, S. Grion, and R. Williams, 2014, Broadband processing of west of Shetland data: First Break, **32**, 97–103.

Wang, P., S. Ray, and K. Nimsaila, 2014, 3D joint deghosting and crossline interpolation for marine single-component streamer data: 84th Annual International Meeting, SEG, Expanded Abstracts, 3594–3598.

Wang, P., S. Ray, C. Peng, Y. Li, and G. Poole, 2013, Premigration deghosting for marine streamer data using a bootstrap approach in Tau-P domain: 83rd Annual International Meeting, SEG, Expanded Abstracts, 4221–4225.

Wu, Q., C. Lee, W. Zhao, P. Wang, and Y. Li, 2014, 3D deghosting for full-azimuth and ultra-long offset marine data: 84th Annual International Meeting, SEG, Expanded Abstracts, 4238–4242.

Zhou, Z., M. Cvetkovic, B. Xu, and P. Fontana, 2012, Analysis of a broadband processing technology applicable to conventional streamer data: First Break, **30**, 77–82.